frontiers in Energy Research

ORIGINAL RESEARCH
published: 02 July 2021
doi: 10.3389/fenrg.2021.689657

Investigation of the S-Shaped Current–Voltage Curve in High Open-Circuit Voltage Ruddlesden–Popper Perovskite Solar Cells

*Hong Zhong, Renlai Zhou, Xiaoqing Wu, Xiaoyun Lin, Ya Wang, Qian Li and Hang Zhou**

School of Electronic and Computer Engineering, Peking University Shenzhen Graduate School, Shenzhen, China

We report our investigation on the S-shaped current–voltage characteristics in a hot-casting–processed $(BA)_2(MA)_3Pb_4I_{13}$ Ruddlesden–Popper (RP) perovskite solar cell. The two-dimensional perovskite solar cells are fabricated with NiO_x as the hole transport layer (HTL), which leads to significantly high open-circuit voltage (V_{oc}). The champion device shows a V_{oc} of 1.21 V and a short current density (J_{sc}) of 17.14 mA/cm^2, leading to an overall power conversion efficiency (PCE) of 13.7%. Although the PCE is much higher than the control device fabricated on PEDOT:PSS, a significant S-shaped current–voltage behavior is observed in these NiO_x-based devices. It is found that the S-shaped current–voltage behavior is related to the lower dimensional phase distribution and crystallinity at the bottom interface of the RP perovskite layer, and the S-shaped distortion is less severe after the device ageing test.

Keywords: low dimension, perovskite solar cell, S-shaped, high V_{oc}, phase distribution, hot casting

OPEN ACCESS

Edited by:
Letian Dou,
Purdue University, United States

Reviewed by:
Jingjing Xue,
University of California, Los Angeles, United States
Yongsheng Liu,
Nankai University, China

****Correspondence:***
Hang Zhou
zhouh81@pkusz.edu.cn

Specialty section:
This article was submitted to Solar Energy, a section of the journal Frontiers in Energy Research

Received: *01 April 2021*
Accepted: *24 May 2021*
Published: *02 July 2021*

Citation:
Zhong H, Zhou R, Wu X, Lin X, Wang Y, Li Q and Zhou H (2021) Investigation of the S-Shaped Current–Voltage Curve in High Open-Circuit Voltage Ruddlesden–Popper Perovskite Solar Cells. Front. Energy Res. 9:689657. doi: 10.3389/fenrg.2021.689657

INTRODUCTION

Metal-halide perovskites have attracted tremendous attention as revolutionary photovoltaic materials owing to their remarkable electronic and optoelectronic properties such as high absorption coefficient, tunable bandgaps, long carrier diffusion length, and solution-processed and low-cost potential. The inherent instabilities of perovskite are becoming a bottleneck for the practical application of perovskite solar cells (PSCs). Recently, two-dimensional (2D) Ruddlesdon–Popper perovskites (RPPs) have become promising alternatives to 3D perovskite in terms of stability. RPPs are conventionally denoted as $(RNH_3)_2A_{n-1}M_nX_{3n+1}$, where RNH_3 represents bulky aliphatic or aromatic alkylammoniums, for example, butylammonium (BA^+), iso-BA^+, and phenethylammonium (PEA^+); A is the cation; M is the metal ion; and X is the halide ion. Their hydrophobic organic spacer cations are resistant to the moisture impregnation (Saparov and Mitzi, 2016; Yang et al., 2016; Etgar, 2018). However, 2D RPP perovskites show restricted charge transport, originated from the quantum and confinement effect of 2D RPP perovskites. The improving stability against the ambient environment in 2D RPP perovskites is therefore at the cost of relatively low performance compared to their 3D counterparts. Fortunately, tremendous efforts have been taken to develop high-performance 2D RPP PSCs. Zhang et al (Wu et al., 2019a) reported the 2D $(BA)_2(MA)_3Pb_4I_{13}$ PSCs with the PCE of 17.26% by developing a slow post-annealing (SPA) process. In 2019, Zhao et al (Ke et al., 2019) broke the PCE records of 2D PSCs by achieving the PCE

of 18.48% for $(GA)(MA)_3Pb_3I_{10}$ perovskite, with improved ambient stabilities. Huang et al. (2021) also reported multifunctional interface engineering by employing guanidinium bromide (GABr) to optimize the secondary crystallization process, realizing a PCE value of 19.3% for 2D PSCs under AM 1.5G illumination. The optimized device without encapsulation could retain 94% of the initial PCE for more than 3,000 h after being stored under ambient conditions.

Further researches on 2D perovskite have revealed that different preparation processes for 2D perovskite show significant effect on the crystallization kinetics and the crystal orientation of the resulted 2D perovskite films. It is widely recognized that crystallization, phase distribution, and orientation profiles of 2D perovskite have critical influences on charge carrier dynamics and thus the performance of PSCs. Tsai et al. systematically researched hot-casting methods in preparing RP PSCs based on the PEDOT:PSS hole transport layer (HTL) and obtained cells with the PCE of 12.51% and V_{oc} of ~1 V (Tsai et al., 2016). Meanwhile, the crystal orientation of 2D perovskite films prepared by hot casting shows a special orientation perpendicular to the glass substrate, which can significantly facilitate efficient charge transport. It has been reported that 2D layered perovskite films cast from perovskite solution precursors with a specific n value are not composed of a single component of n-layered 2D perovskites but rather a mixture of 2D perovskites with various thicknesses (*n*) (Quintero-Bermudez et al., 2018). For the hot-casting process, generally speaking, in the obtained 2D perovskite film, the larger n phase is preferentially distributed on the top of the film, which tends to be perpendicular to the substrate; the middle part is multi-n phase; and the small n phase is more likely distributed on the bottom of the film, which tends to be parallel to the substrate (Xu et al., 2020). This gradient phase distribution in the 2D perovskite film is conductive to the alignment of the energy bands and facilitates the energy transfer of excitons, and thus the transmission of carriers. Researchers have reported high-quality 2D perovskite films through the hot-casting method, and thus demonstrated high-performance PSCs, but it is worthily noted that most of the common structures reported of inverted quasi-2D RP PSCs are using PEDOT:PSS or PTAA as the hole transport layer (HTL). Unlike the 3D counterpart, 2D PSCs based on nickel oxide (NiO_x) hole transport material are rarely reported, probably due to the S-shaped behavior in the current–voltage characteristics discussed in this work (Chen et al., 2018; Boyd et al., 2020; Liang et al., 2021). Chen et al. fabricated 2D PSCs based on $BA_2MA_2Pb_3I_{10}$, and using a NiO_x HTL and a PCBM (50wt% ICBA) mix ETL. In this structure, 2D PSCs demonstrated a PCE of 12.07% with a V_{oc} of 1.23 V. The author indicated that the decreasing energy loss at the interface between NiO_x and n = 3 2D perovskite was revealed, which attributed to the enhanced V_{oc}.

Here, we report a hot-casting–processed 2D RP PSC based on 2D $(BA)_2(MA)_3Pb_4I_{13}$ (n = 4) layered perovskite films fabricated with an inverted structure using NiO_x as the hole transport layer (HTL). With the NiO_x HTL, the RP PSC shows significantly enhanced open-circuit voltage (V_{oc}) compared to devices derived from PEDOT:PSS or PTAA. Our champion device ($FTO/NiO_x/(BA)_2(MA)_3Pb_4I_{13}$/PCBM/BCP/Ag) has shown a V_{oc} of 1.21 V under standard AM 1.5G illumination, which is one of the highest records among recent researches on inverted 2D RPPs PSCs. We observed an S-shaped behavior in the I-V characteristics of our 2D RP PSCs. To investigate the differences of 2D perovskite films based on different substrates, powder X-ray diffraction (XRD) has been adopted, indicating that the enhanced crystal orientation of 2D perovskite flakes upon NiO_x-based devices. Spatially resolved photoluminescence (PL) measurements show that a gradient phase distribution from top to bottom is consistent with literature reports, and NiO_x-based devices exhibit a favorable alignment on the multiple perovskite phases and lower trap states of 2D perovskite flakes. We also performed transient absorption (TA) techniques to compare the charge carrier dynamics in layered perovskite films based on NiO_x and PEDOT:PSS, further confirming the efficient charge carrier funneling from small-n to large-n 2D phases inside the film, and it is found that a faster charge transfer and suppressed charge recombination occurred in the NiO_x-based devices due to a more enhanced alignment profile of multiple phases of 2D perovskite component, resulting in a higher V_{oc}.

RESULTS AND DISCUSSION

The 2D perovskite film with a formula of $(BA)_2(MA)_3Pb_4I_{13}$ by using the hot-casting method and subsequent fabrication of inverted PSCs with a structure of NiO_x or PEDOT:PSS)/ $(BA)_2$ $(MA)_3Pb_4I_{13}$ /PCBM/BCP/Ag, as shown in **Figures 1A,B**, shows the comparison of performance of the fabricated 2D RPP perovskite solar cells derived from NiO_x and PEDOT:PSS. Both devices exhibited relatively high performance relative to those reported records with the similar structure. Intriguingly, *via* further tests, we observed that the photovoltaic performance of the BA-based 2D PSCs improves after several days storage (ageing) in the glove box, as shown in **Figure 1B**. After ageing, for the controlled PEDOT:PSS–based devices, we achieved a champion PCE value of 11.0%, a J_{sc} of 16.98 mA/cm^2, and a V_{oc} of 0.95 V. The NiO_x-based devices exhibited a remarkable improvement of V_{oc} up to 1.2 V and J_{sc} of 17.14 mA/cm^2; as a result, the much improved V_{oc} and slightly improved J_{sc} led to an overall PCE of 13.7%. Interestingly, it was found that the J–V curves of the NiO_x-based device in **Figure 1B** exhibit an "S" shape around the open-circuit voltage position, resulting in a higher V_{oc} value and a relatively lower fill factor (FF). Moreover, we found that this phenomenon occurred in the NiO_x-based PSCs varied during the ageing test, as shown in **Figure 2**.

In our work, we used the differential coefficient k at the V_{oc} point to evaluate the "S"-shaped curve, with a smaller k indicating severer degree of distortion. According to **Figure 2**, the value of k1 is summarized at **Supplementary Table S1**. It is shown that the k value of the corresponding J–V curve increased from 57.93 to 68.97 for the NiO_x-based PSC during the ageing test. The performance of the PSC was enhanced in this process.

Figures 3A–D show the distribution of photovoltaic parameters (V_{oc}, J_{sc}, FF, and PCE) of devices derived from

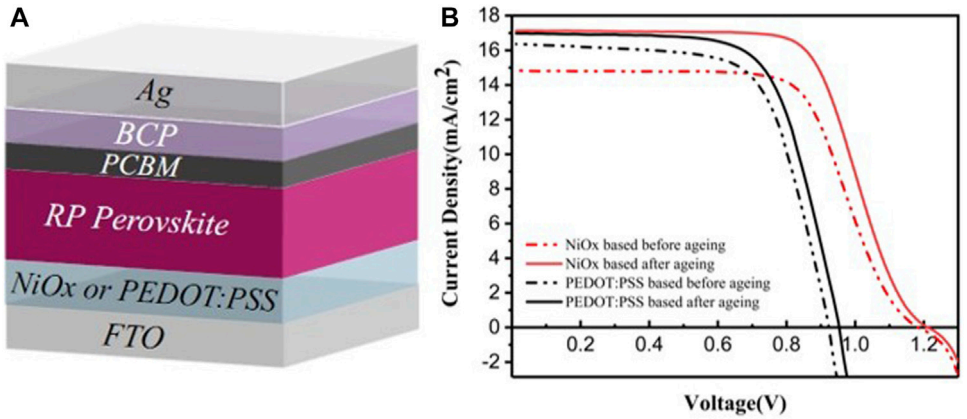

FIGURE 1 | (A) Device architecture of the PSCs. **(B)** J–V characteristics of device A (NiO_x-based PSCs) and device B (PEDOT:PSS–based PSCs).

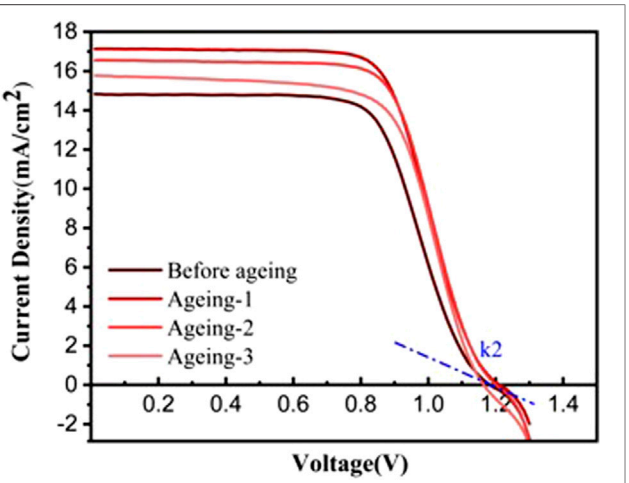

FIGURE 2 | J–V curves of NiO_x-based PSCs in different ageing states.

different HTLs. The statistical data were obtained from ~15 cells. As illustrated in **Figure 3**, the major improvement lies in the increased V_{oc} and more uniform J_{sc} and FF distribution. The external quantum efficiency (EQE) of different HTL devices is shown in **Supplementary Figure S1**. Note that after the ageing test, the EQE values of NiO_x-based and PEDOT:PSS–based devices are significantly enhanced, matching the promoted short current density in J–V curves after ageing, as shown above. The improved J_{sc} and EQE could be due to an improved contact between the perovskite and HTLs, the exact mechanism of which requires further investigation. To further the investigation, dark current density–voltage (J–V) characteristics of different HTL devices before and after ageing was performed, as shown in **Supplementary Figure S2**. The significant reduction of the leakage current for all samples after ageing is an indication of suppression of carrier recombination (Du et al., 2019).

X-ray diffraction (XRD) measurements were carried out for perovskite films deposited on FTO glass/NiO_x and PEDOT:PSS substrates, as illustrated in **Supplementary Figure S4**. Diffraction peaks at around 14.1° and 28.3°in the XRD pattern are ascribed to the (111) and (202) crystallographic planes, respectively. The intensity of the diffraction peaks for both films is consistent with that reported previously on hot-casting methods (Tsai et al., 2016). Furthermore, for the NiO_x-based device, the increase of the intensity for (111) peak is observed, indicating an improved growth quality in (111) direction.

The cross-sectional scanning electron microscopy (SEM) measurements were performed to figure out the effect of the HTL substrate on 2D perovskite films' morphology, as shown in **Supplementary Figure S5**. NiO_x- and PEDOT:PSS–based samples exhibited a similar smooth and pin-hole free surface, with bricklike grains.

It has been suggested that the phase distribution in 2D perovskite films plays an important role in the efficiency of photovoltaic devices. We speculated that the substrates with different HTLs may affect the phase formation in 2D layered perovskite films. The perovskite film composition and phase distribution are therefore investigated in order to explain the differences between devices derived from NiO_x and PEDOT:PSS. **Supplementary Figure S3** shows light absorption of perovskite layers and different HTLs on FTO. The 2D RP perovskite spin coated on NiO_x presented slightly higher absorbance than that on the PEDOT:PSS device. Moreover, peaks representing n = 2, 3, and 4 can be observed, which suggests that the 2D RPP perovskite film consists of multiple phases containing different n, it is consistent with that reported previously.

The steady-state photoluminescence (PL) spectroscopy measurements were collected with an excitation wavelength of 450 nm from both the front- (perovskite film side) and back-side (substrate side) illumination to reveal the spatial phase composition of the as-fabricated 2D-RPP films based on different HTLs (NiO_x and PEDOT:PSS). With an excitation wavelength of 450 nm, the penetration depth into layered perovskite films can be estimated to be ~150 nm based on the absorption spectra, which is smaller than the film thickness of ~350 nm, indicating that the fluorescence signals collected are

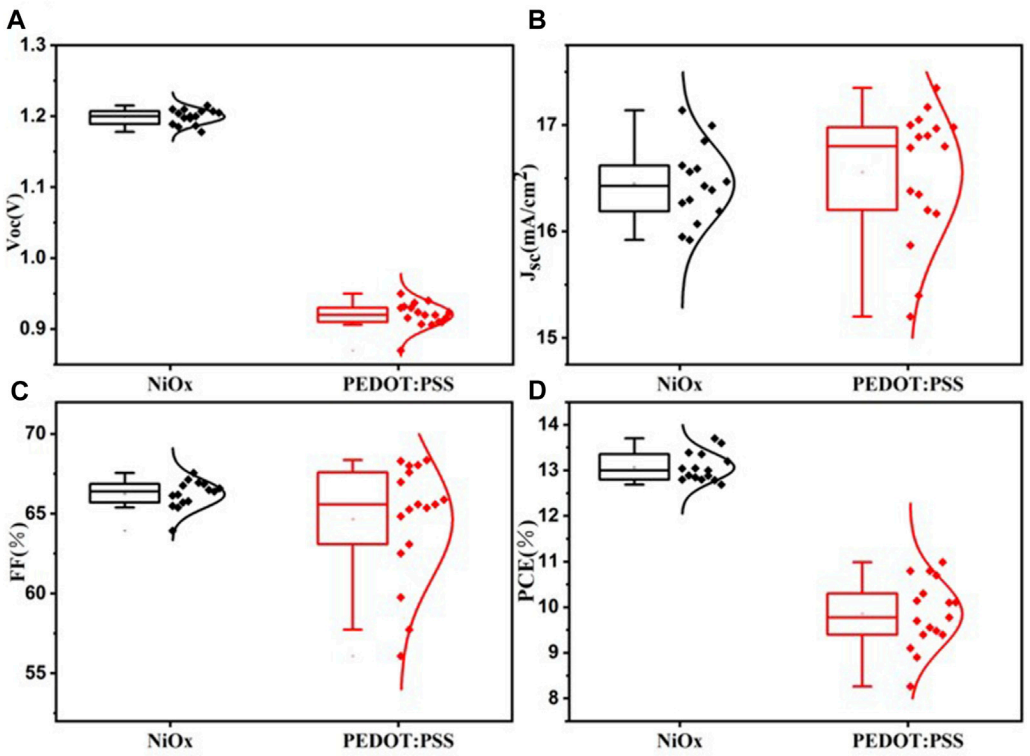

FIGURE 3 | Dependence of photovoltaic parameters of the NiO_x- and PEDOT:PSS–based perovskite devices. The data were statistically analyzed from ~15 cells.

mainly from the same side of films as the photoexcitation (Jang et al., 2020).

In pristine films (before ageing), when excited from the back side (glass side), a dominant long-wavelength PL peak and additional multiple emission peaks at shorter wavelength were detected. According to previous reports, short-wavelength PL peaks in **Figure 4A** can be assigned to emission of 2D perovskite crystals with small-n phases. The emission peaks at 578 nm, 610 nm, and 640 nm are corresponding to n = 2, 3, and 4, respectively. The dominant peak at the long wavelength can be assigned to the 3D-like perovskite. In contrast, as shown in **Figure 4B**, the PL spectra obtained from the front-side excitation only demonstrated a dominant emission peak at ~740 nm; the dominant peak in **Figure 4B** at the long wavelength is due to the large-n (3D-like) perovskite component. This result indicates that small-n phases mainly locate at the substrate (NiO_x and PEDOT:PSS) side, and the large-n phases majorly distribute in the upper surface of the films. This phase distribution is beneficial to the self-driven charge separation and transport (from the small-n region to large-n region) in 2D perovskite films (Du et al., 2019). The PL intensity ratio between different emission peaks suggested that the distribution of different phases of layered perovskites was not uniform along the out-of-plane direction in the film. Note that in **Figure 4B**, in the front-side excitation, the emission peak of the NiO_x-based sample shifts toward longer wavelength, compared to the PEDOT:PSS–based sample, indicating the improvement of film quality with better crystallization of 3D-like components on the top of the 2D perovskite film (Lian et al., 2019; Meng et al., 2020; Zheng et al., 2020a; Zheng et al., 2020b). Furthermore, the higher PL intensity of emission peaks to the 3D-like component in the NiO_x-based perovskite film from both side excitation indicates the increased crystallinity of 3D-like perovskite phases and the decreased defect state density, compared to PEDOT:PSS–based films (Zheng et al., 2019; Zheng et al., 2020a). However, in **Figure 4A**, in the back-side excitation, the steady-state PL is enhanced more strongly in the NiO_x-based film, revealing impeditive hole transmission in the NiO_x/perovskite surface, and thus causes charge recombination. In addition, compared with the PEDOT:PSS–based perovskite film, it can be found that the intensities of emission peaks at low-n phases considerably enlarge relative to the 3D phase peak in the NiO_x-based one, indicating the better crystallization and more 2D phases deposited at the bottom of the NiO_x-based film (Wu et al., 2019a).

We can also find that the PL peaks of different phases enhanced after ageing, as shown in **Figure 4**, indicating an increased crystallinity for both 2D and 3D perovskite phases in the thin film after ageing, and this enhancement is more observable in the NiO_x-based film than in the PEDOT:PSS–based film. This variation of peak intensity of low-n phases in back excitation can be more detectable in **Supplementary Figure S6**. Moreover, the emission peak position of the large-n perovskite phase in the NiO_x- and PEDOT:PSS–based perovskite film varied from ~744 nm and ~741 nm to ~740 nm and ~737 nm, respectively. The blue shift of the PL emission resulted from a

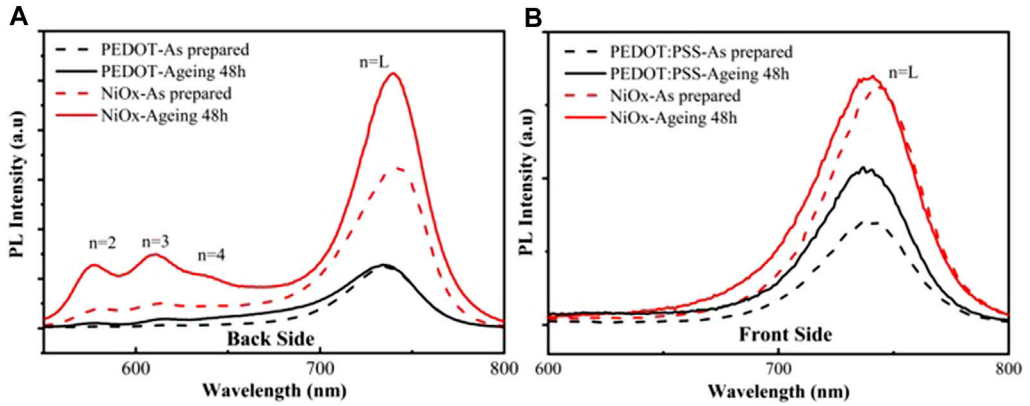

FIGURE 4 | Steady-state PL spectra of films before ageing. **(A)** Back excitation and **(B)** front excitation.

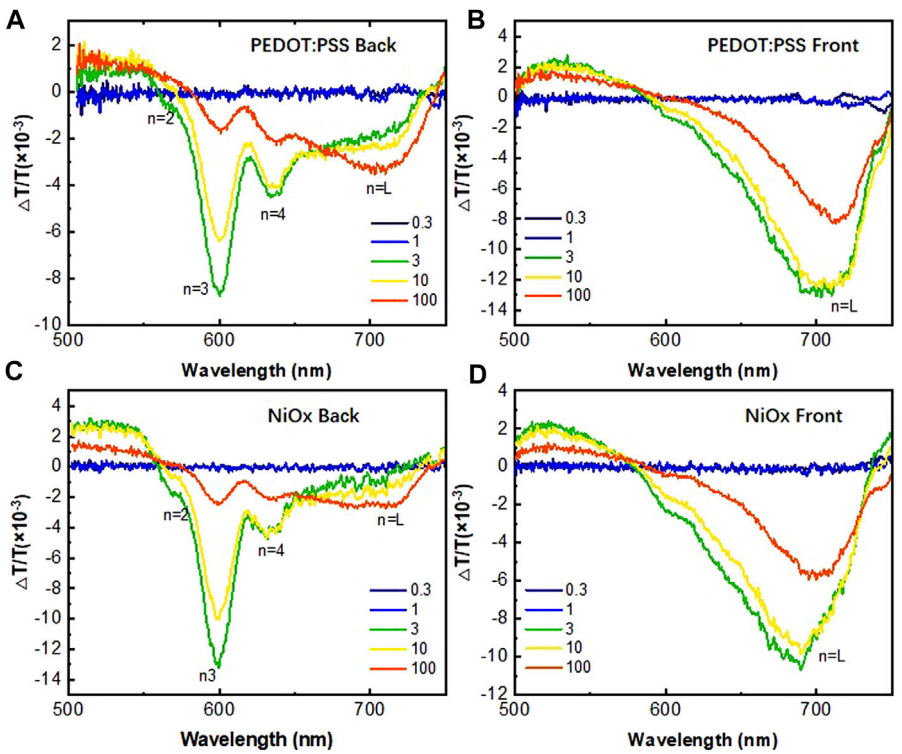

FIGURE 5 | (A) TA spectra of PEDOT:PSS–based samples from back-side excitation and **(B)** front-side excitation. **(C)** TA spectra of NiO_x-based samples from back-side excitation and **(D)** front-side excitation.

reduced trap density within the 3D-like perovskite after ageing (Chen et al., 2018; Xu et al., 2019; Huang et al., 2021).

Ultrafast transient absorption (TA) measurements were also carried out to further probe the compositional change and carrier dynamic of layered perovskite films upon different substrates, as shown in **Figure 6**. In order to probe the vertical distribution change of perovskite films, the excitation laser was beamed from the back side (FTO substrate) and from the front side (surface of the perovskite), and the 2D perovskite films have been ageing for 160 h, as shown in **Figures 5A–D**, respectively. In the transient absorption spectra (ΔT/T), negative signals correspond to ground-state bleaching (GSB). In all cases, a positive weak and broad signal at wavelengths shorter than 600 nm can be observed, which can be assigned to the derivative feature resulting from the blue shift of the band-edge exciton resonance predominantly from the $n = 3$ phase (Wu et al., 2015). Distinct GSB peaks can be easily recognized in the TA spectra. Both the TA spectra of the 2D RPP perovskite film derived from two kinds of HTL devices

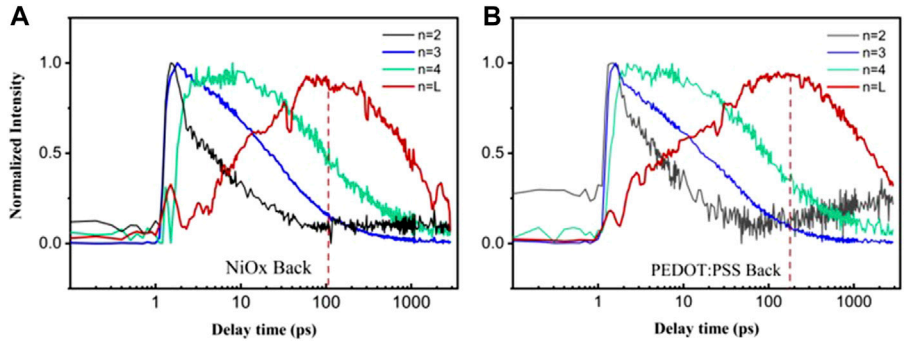

FIGURE 6 | TA kinetics probed at bleach peaks of various n values of the **(A)** PEDOT:PSS–based film and the **(B)** NiO_x-based film.

exhibit GSB peaks corresponding to phases of n = 2,3,4, and ∞. We can find drastic differences in the TA spectra with opposite excitation, where lower n (n = 3,4) dominated the back-excitation TA spectra. In contrast, with front excitation, GSB of n = ∞ becomes significantly stronger. These results further confirm that upon the hot-casting process, perovskite tends to crystallize first on the surface, which leads to 3D component to preferentially nucleate first on the surface while 2D components are preferentially segregated at the bottom; this naturally results in the gradient distribution of the QW in the film. This vertical distribution of different perovskite phases allows effective energy transfer from small-n phases to larger-n phases, followed by charge transport to the corresponding electrodes *via* the cascaded energy levels. It can be found that from the back-site excitation, the intensities of the n = 3 phase peak are significantly higher and the GSB of the n = ∞ phase is weaker in the NiO_x-based film than those in the PEDOT:PSS–based film. It is speculated that films deposited on NiO_x contain more lower dimension perovskite composition, which is consistent with the PL measurement discussed above, giving a more favorable energy landscape for the faster charge/energy transfer process.

To obtain the transport dynamics of excitons and carriers in layered perovskite films, the TA signals as a function of pump-probe delay at wavelengths of each GSB peak from back excitation of both samples are plotted in **Figure 6**. The decay profiles of small-n phases can be attributed to a combined process for exciton decay, including radiative recombination, trap-state filling, and energy transfer to the large-n phase. The rise of the GSB signal of the large-n phase has been previously assigned to the progressive population of excitons in the large-n perovskite phase due to energy transfer from small-n perovskites. Therefore, the GSB signal corresponding to the large-n phase goes on to a decay process on the nanosecond timescale. It is found that the decrease of GSB signals of lower-n phases is followed by GSB peaks at larger-n (~715 nm). It implies that the sequence in which the cross peaks grow suggests a cascade of energy transfer event from higher energy (low-n) phases to lower energy phases (high-n) in quasi-2D RP perovskite films. Such an energy cascade from a low-n phase to a high-n phase promotes self-driven charge separation and transportation, which is beneficial to the PSC performance (Liu et al., 2017). It can be found that, in **Figure 6**, the low-energy bleach (n = L phase) reaches a maximum magnitude of signal (103.8 ps), which is much faster than that in **Figure 6** (185.1 ps), implying faster energy transfer from the low-n phase to the high-n phase.

In the hot-casted quasi-2D RP perovskites, multiple phases of perovskites are distributed in vertical direction from small to large n and coexist randomly at the bottom of the perovskite thin film (Bube, 1962; Zheng et al., 2019). Lin et al. reported that 2D perovskite $(BA)_2(MA)_3Pb_4I_{13}$ thin films comprise multiple layered (small-n) perovskite phases surrounded by 3D-like (large-n) phases (Lin et al., 2019). According to this landscape of phase distribution of the 2D RPP perovskite film, excitons and charge carrier transport mechanism have been unveiled (Lin et al., 2020). It is speculated that energy transfer from the larger bandgap layered perovskites to lower bandgap 3D-like perovskites across the ligands at a very early delay timescale. Generally, the layered flakes are few layers in the 2D RP perovskite film, thus most of excited carriers would be transferred to 3D phase perovskites. After energy transfer, excitons will dissociate into free charge carriers quickly due to the small exciton binding energy in 3D-like perovskite. The collected charge carriers sequentially transport within 3D phase networks with their advantageous high carrier mobilities and long carrier lifetimes. The excitons and charge carrier transport mechanism can be illustrated in **Figure 7A**.

In the case of the RP 2D phase perovskite, the QW width largely affects the Eg, which is determined by the basic 3D structure and additional quantization due to 2D confinement of the electron–hole pair. The optical bandgap of the 2D perovskite with general formula $L_2A_{n-1}B_nX_{3n+1}$ depends on the value of n, and bandgap decreases as the value of n increases due to the quantum and dielectric confinement (Cao et al., 2015; Sichert et al., 2015; Mao et al., 2017; Stoumpos et al., 2017; Gao et al., 2018). For the BA-based RP perovskite, it has been revealed that the optical bandgap increased from 1.52 to 2.24 eV with decreasing n from 5 to 1 (Blancon et al., 2017). The energy diagram of our PSCs can be illustrated at **Figure 7B**. The values of the valence band (VB) and conduction band (CB) were adopted from the literature, which were calculated *via* ultraviolet

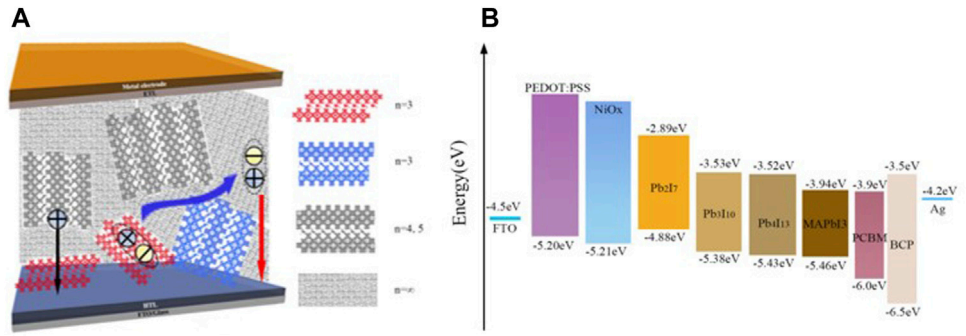

FIGURE 7 | (A) Excitations and charge carrier transport mechanism in the 2D RPP perovskite film. **(B)** Energy diagram for devices with inverted PSC configuration.

photoelectron spectroscopy (UPS) (Cao et al., 2015; Stoumpos et al., 2016; Liu et al., 2017).

In the above measurement, steady-state PL measurements confirm that a graded vertical phase distributed across the film, where 3D-like phase was preferred to form on the top of the film, whereas low-n phases coexist at the bottom. The NiO_x-based perovskite film shows a higher proportion of low-n phases at the bottom than the PEDOT:PSS–based film. Reports have shown that those $n < 3$ perovskite flakes are more likely oriented with their inorganic slabs parallel to the substrate (Shao et al., 2019); in addition, the insulating nature of the chain organic cation and the quantum confinement effect also inhibit the charge transport in the vertical direction, acting as a role of carrier transport barrier (black arrow in **Figure 7A**), and carriers can only transport to the HTL through the surrounding 3D-like perovskite framework around 2D flakes in the bottom of the 2D perovskite film (red arrow in **Figure 7B**) (Lin et al., 2019), resulting in low current density in the resulted PSCs (**Figure 1B**). After ageing for 48 h, the enhanced PL peaks and the blue shift of the emission peak of 3D-like component indicated better crystallization and lower trap-state density for both 2D and 3D phases in 2D perovskite films, promoting the performance of 2D PSCs.

With further ageing for 160 h, ultrafast transient absorption spectra revealed a faster energy transfer process in the NiO_x-based perovskite film, which can be attributed to a more favorable energy landscape. To sum up, the ageing effect on the 2D RPP perovskite film can be ascribed to enhanced crystallinity and decreased trap-state density. When preparing the 2D perovskite film with the hot-casting process, due to the preheated substrate, the intermediate between solvent molecules and PbI_2 changes quickly and consumes a lot of organic cations in the bottom of the perovskite film, resulting in the gradient distribution of the QW in the film (Xu et al., 2020). After this rapid crystallization process, low-n phases of 2D perovskite are formed in the bottom of the pristine film with relatively low crystallinity and random orientation (Chen et al., 2019). In terms of the results of PL and TA measurements, we speculated that during the ageing test, with the effect of thermal stress and light soaking, the 2D perovskite happened to recrystallize gradually, resulting in better crystallinity and preferential orientation. Consequently, enhanced performance of PSCs was found after the ageing test.

V_{oc} is related to the losses *via* radiative recombination (due to spectral mismatch) and non-radiative recombination involving traps or interfacial misalignment (Wu et al., 2019b). To summarize, the V_{oc} enhancement in this work is attributed to a more favorable alignment of multi-perovskite phases in the order of n values along the vertical direction perpendicular to the substrate in the NiO_x-based RPP perovskite film (Wu et al., 2019a), which can facilitate charge transport with suppressed recombination. The voltage loss *via* non-radiative recombination is therefore mitigated. The ageing operation can induce better crystallinity and reduced defect density, which facilitate PSC performance.

The S-shaped I-V curves were frequently observed in silicon heterojunction (SHJ) solar cells, CdTe, copper indium (gallium) selenide [CI(G)S], a-Si, and even perovskite cells. It has been suggested that the S-shaped I-V curves were linked to a mismatch between the energy levels of the absorber layer and the charge extraction layers, leading to a barrier for charge extraction (Wu et al., 2019b). Moreover, these barriers can be created through a mismatch in band alignment between the absorber layer and the selective contact or the passivation layer. The S-shaped deformation in the J–V characteristic is rarely reported in 2D RPP PSCs. As shown in **Figure 7B**, the valence band maximum (VBM) of 2D BA-based $n = 2$ RP perovskites is set at 4.88 eV, and the VBM of both NiO_x (~5.21 eV) and PEDOT:PSS (~5.2 eV) is too deep for holes to be extracted. It is clearly calculated that the energy-level offset (ΔE) for charge transfer between the VBM of NiO_x/PEDOT:PSS and $n = 2$ perovskite is 0.32 eV, which is of paramount interest to the devices' J–V characteristic (Schulz et al., 2014). Thus, we deduce that the scenario of the S-shaped deformation at the V_{oc} point is aroused by the energy-level offset between the NiO_x and low-dimensional perovskite, causing partial band bending on the surface of p/i heterojunction, and thus impeding energy transfer and hole transportation (Aghassi et al., 2018; Li et al., 2018; Saive, 2019; Boyd et al., 2020). According to the results of PL and TA measurements, for NiO_x-based PSCs, with further ageing, 2D components at the bottom of the perovskite film started to recrystallize, forming high crystalline $n = 2$, $n = 3$, and $n = 4$ phases. The VBM of perovskite further decreased to match the

VBM of the NiO_x layer, and thus, the energy barrier for hole transport was reduced, leading to enhanced performance of PSCs, and the S-shaped deformation in J–V curves gradually vanished. These profiles and results are in line with the variation of J–V curves and the parameter k1, as shown in **Figure 2** and **Supplementary Table S1**.

To sum up, we have fabricated a high V_{oc} (1.2 V) inverted 2D RP PSCs by the hot-casting method and achieved a power conversion efficiency of 13.7%. Investigations were carried out to explain the difference between devices of two kinds of the HTL. The NiO_x-based 2D layered PSCs possess better phase distribution and crystallinity, and thus resulting in faster charge transmission and lower trap states, resulting in a higher V_{oc} than their counterparts. Moreover, a hole transport barrier between the HTL and perovskite surface, which is the cause of the deformation near the V_{oc} position, was observed. The origin of this effect needs further investigation; we believed that this observation is beneficial to further evolve the strategies for fabricating large V_{oc} and high-performance 2D RP perovskite PSCs.

EXPERIMENTAL METHODS

Device Fabrication and Characterizations

Pre-patterned FTO glass plates were sequentially cleaned by ultrasonication in deionized water, acetone, and isopropyl alcohol for 15 min. After 15 min of UV ozone treatment, different hole transporting layers were deposited on the FTO substrate. For NiO_x-based PSCs, NiO_x was spin-coated on FTO at 2,000 rpm for 30 s and annealed in air for 5 min at 180°C; this step was repeated for three times, and then, FTO coated with NiO_x was annealed in air for 2 h at 480°C. For PEDOT:PSS–based PSCs, poly(3,4-ethylenedi-oxythiophene):polystyrene sulfonate (PEDOT:PSS) was spin-coated on FTO at 2,000 rotations per minute (rpm) for 60 s and annealed in air at 150°C for 20 min. Lately, a 2D RPP perovskite thin film with a formula of (BA)2(MA)3Pb4I13 was spin-coated on the coated substrate, utilizing the hot-casting process as reported by Tsai et al. (9), and we set our hot-casting temperature at 130°C. A PCBM electron transporting layer was then sequentially spin-coated on the top of layered perovskite films using PCBM (20 mg/ml in chlorobenzene) at 2,000 rpm for 30 s. BCP (0.5 mg/ml in ethyl alcohol) was then spin-coated on PCBM at 2,000 rpm for 60 s, followed by deposition of 120 nm Ag.

DATA AVAILABILITY STATEMENT

The original contributions presented in the study are included in the article/**Supplementary Material**; further inquiries can be directed to the corresponding author.

AUTHOR CONTRIBUTIONS

HoZ is the dominant researcher, and HaZ is the adviser.

ACKNOWLEDGMENTS

This work was financially supported by the Guangdong Natural Science Foundation (2018A030313332) and the Shenzhen Municipal Scientific Program (JCYJ20200109140610435 and ZDSYS201802061805105).

SUPPLEMENTARY MATERIAL

The Supplementary Material for this article can be found online at: https://www.frontiersin.org/articles/10.3389/fenrg.2021.689657/full#supplementary-material

REFERENCES

Aghassi, A., Fay, C. D., and Mozer, A. (2018). Investigation of S-Shaped Current-Voltage Characteristics in High-Performance Solution-Processed Small Molecule Bulk Heterojunction Solar Cells. *Org. Electron.* 62, 133–141. doi:10.1016/j.orgel.2018.07.025

Blancon, J.-C., Tsai, H., Nie, W., Stoumpos, C. C., Pedesseau, L., Katan, C., et al. (2017). Extremely Efficient Internal Exciton Dissociation through Edge States in Layered 2D Perovskites. *Science* 355 (6331), 1288–1292. doi:10.1126/science.aal4211

Boyd, C. C., Shallcross, R. C., Moot, T., Kerner, R., Bertoluzzi, L., Onno, A., et al. (2020). Overcoming Redox Reactions at Perovskite-Nickel Oxide Interfaces to Boost Voltages in Perovskite Solar Cells. *Joule* 4 (8), 1759–1775. doi:10.1016/j.joule.2020.06.004

Bube, R. H. (1962). Trap Density Determination by Space-Charge-Limited Currents. *J. Appl. Phys.* 33 (5), 1733–1737. doi:10.1063/1.1728818

Cao, D. H., Stoumpos, C. C., Farha, O. K., Hupp, J. T., and Kanatzidis, M. G. (2015). 2D Homologous Perovskites as Light-Absorbing Materials for Solar Cell Applications. *J. Am. Chem. Soc.* 137 (24), 7843–7850. doi:10.1021/jacs.5b03796

Chen, A. Z., Shiu, M., Deng, X., Mahmoud, M., Zhang, D., Foley, B. J., et al. (2019). Understanding the Formation of Vertical Orientation in Two-Dimensional Metal Halide Perovskite Thin Films. *Chem. Mater.* 31 (4), 1336–1343. doi:10.1021/acs.chemmater.8b04531

Chen, J., Lian, X., Zhang, Y., Yang, W., Li, J., Qin, M., et al. (2018). Interfacial Engineering Enables High Efficiency with a High Open-Circuit Voltage above 1.23 V in 2D Perovskite Solar Cells. *J. Mater. Chem. A.* 6 (37), 18010–18017. doi:10.1039/c8ta06925e

Du, X., Qiu, R., Zou, T., Chen, X., Chen, H., and Zhou, H. (2019). Enhanced Uniformity and Stability of Pb-Sn Perovskite Solar Cells via Me 4 NBr Passivation. *Adv. Mater. Inter.* 6 (14), 1900413. doi:10.1002/admi.201900413

Etgar, L. (2018). The merit of Perovskite's Dimensionality; Can This Replace the 3D Halide Perovskite? *Energy Environ. Sci.* 11 (2), 234–242. doi:10.1039/c7ee03397d

Gao, P., Bin Mohd Yusoff, A. R., and Nazeeruddin, M. K. (2018). Dimensionality Engineering of Hybrid Halide Perovskite Light Absorbers. *Nat. Commun.* 9 (1), 5028. doi:10.1038/s41467-018-07382-9

Huang, Y., Li, Y., Lim, E. L., Kong, T., Zhang, Y., Song, J., et al. (2021). Stable Layered 2D Perovskite Solar Cells with an Efficiency of over 19% via Multifunctional Interfacial Engineering. *J. Am. Chem. Soc.* 143 (10), 3911–3917. doi:10.1021/jacs.0c13087

Jang, G., Ma, S., Kwon, H.-C., Goh, S., Ban, H., Kim, J. S., et al. (2020). Elucidation of the Formation Mechanism of Highly Oriented Multiphase Ruddlesden-Popper Perovskite Solar Cells. *ACS Energ. Lett.* 6, 249–260. doi:10.1021/acsenergylett.0c02438

Ke, W., Mao, L., Stoumpos, C. C., Hoffman, J., Spanopoulos, I., Mohite, A. D., et al. (2019). Compositional and Solvent Engineering in Dion-Jacobson 2D Perovskites Boosts Solar Cell Efficiency and Stability. *Adv. Energ. Mater.* 9 (10), 1803384. doi:10.1002/aenm.201803384

Li, X., Shen, K., Li, Q., Deng, Y., Zhu, P., and Wang, D. (2018). Roll-over Behavior in Current-Voltage Curve Introduced by an Energy Barrier at the Front Contact in Thin Film CdTe Solar Cell. *Solar Energy* 165, 27–34. doi:10.1016/j.solener.2018.02.075

Lian, X., Chen, J., Qin, M., Zhang, Y., Tian, S., Lu, X., et al. (2019). The Second Spacer Cation Assisted Growth of a 2D Perovskite Film with Oriented Large Grain for Highly Efficient and Stable Solar Cells. *Angew. Chem. Int. Ed.* 58 (28), 9409–9413. doi:10.1002/anie.201902959

Liang, J., Zhang, Z., Zheng, Y., Wu, X., Wang, J., Zhou, Z., et al. (2021). Overcoming Carrier Transport Limitation in Ruddlesden–Popper Perovskite Films by Lamellar Nickel Oxide Substrate. *J. Mater. Chem. A* 89, 11741–11752. doi:10.1039/d1ta01038g

Lin, D., Ma, L., Ni, W., Wang, C., Zhang, F., Dong, H., et al. (2020). Unveiling Hot Carrier Relaxation and Carrier Transport Mechanisms in Quasi-Two-Dimensional Layered Perovskites. *J. Mater. Chem. A.* 8 (47), 25402–25410. doi:10.1039/d0ta09530c

Lin, Y., Fang, Y., Zhao, J., Shao, Y., Stuard, S. J., Nahid, M. M., et al. (2019). Unveiling the Operation Mechanism of Layered Perovskite Solar Cells. *Nat. Commun.* 10 (1), 1008. doi:10.1038/s41467-019-08958-9

Liu, J., Leng, J., Wu, K., Zhang, J., and Jin, S. (2017). Observation of Internal Photoinduced Electron and Hole Separation in Hybrid Two-Dimentional Perovskite Films. *J. Am. Chem. Soc.* 139 (4), 1432–1435. doi:10.1021/jacs.6b12581

Mao, L., Wu, Y., Stoumpos, C. C., Traore, B., Katan, C., Even, J., et al. (2017). Tunable White-Light Emission in Single-Cation-Templated Three-Layered 2D Perovskites (CH3CH2NH3)4Pb3Br10-xClx. *J. Am. Chem. Soc.* 139 (34), 11956–11963. doi:10.1021/jacs.7b06143

Meng, J., Song, D., Huang, D., Li, Y., Li, Y., Maqsood, A., et al. (2020). Enhanced VOC of Two-Dimensional Ruddlesden-Popper Perovskite Solar Cells Using Binary Synergetic Organic Spacer Cations. *Phys. Chem. Chem. Phys.* 22 (1), 54–61. doi:10.1039/c9cp04018h

Quintero-Bermudez, R., Gold-Parker, A., Proppe, A. H., Munir, R., Yang, Z., Kelley, S. O., et al. (2018). Compositional and Orientational Control in Metal Halide Perovskites of Reduced Dimensionality. *Nat. Mater* 17 (10), 900–907. doi:10.1038/s41563-018-0154-x

Saive, R. (2019). S-shaped Current-Voltage Characteristics in Solar Cells: A Review. *IEEE J. Photovoltaics* 9 (6), 1477–1484. doi:10.1109/jphotov.2019.2930409

Saparov, B., and Mitzi, D. B. (2016). Organic-Inorganic Perovskites: Structural Versatility for Functional Materials Design. *Chem. Rev.* 116 (7), 4558–4596. doi:10.1021/acs.chemrev.5b00715

Schulz, P., Edri, E., Kirmayer, S., Hodes, G., Cahen, D., and Kahn, A. (2014). Interface Energetics in Organo-Metal Halide Perovskite-Based Photovoltaic Cells. *Energ. Environ. Sci.* 7 (4), 1377. doi:10.1039/c4ee00168k

Shao, S., Duim, H., Wang, Q., Xu, B., Dong, J., Adjokatse, S., et al. (2019). Tuning the Energetic Landscape of Ruddlesden-Popper Perovskite Films for Efficient Solar Cells. *ACS Energ. Lett.* 5 (1), 39–46. doi:10.1021/acsenergylett.9b02397

Sichert, J. A., Tong, Y., Mutz, N., Vollmer, M., Fischer, S., Milowska, K. Z., et al. (2015). Quantum Size Effect in Organometal Halide Perovskite Nanoplatelets. *Nano Lett.* 15 (10), 6521–6527. doi:10.1021/acs.nanolett.5b02985

Stoumpos, C. C., Cao, D. H., Clark, D. J., Young, J., Rondinelli, J. M., Jang, J. I., et al. (2016). Ruddlesden-Popper Hybrid Lead Iodide Perovskite 2D Homologous Semiconductors. *Chem. Mater.* 28 (8), 2852–2867. doi:10.1021/acs.chemmater.6b00847

Stoumpos, C. C., Soe, C. M. M., Tsai, H., Nie, W., Blancon, J.-C., Cao, D. H., et al. (2017). High Members of the 2D Ruddlesden-Popper Halide Perovskites: Synthesis, Optical Properties, and Solar Cells of (CH3(CH2)3NH3)2(CH3NH3)4Pb5I16. *Chem* 2 (3), 427–440. doi:10.1016/j.chempr.2017.02.004

Tsai, H., Nie, W., Blancon, J.-C., Stoumpos, C. C., Asadpour, R., Harutyunyan, B., et al. (2016). High-efficiency Two-Dimensional Ruddlesden-Popper Perovskite Solar Cells. *Nature* 536 (7616), 312–316. doi:10.1038/nature18306

Wu, G., Li, X., Zhou, J., Zhang, J., Zhang, X., Leng, X., et al. (2019a). Fine Multi-phase Alignments in 2D Perovskite Solar Cells with Efficiency over 17% via Slow Post-Annealing. *Adv. Mater.* 31 (42), e1903889. doi:10.1002/adma.201903889

Wu, G., Zhou, J., Zhang, J., Meng, R., Wang, B., Xue, B., et al. (2019b). Management of the Crystallization in Two-Dimensional Perovskite Solar Cells with Enhanced Efficiency within a Wide Temperature Range and High Stability. *Nano Energy* 58, 706–714. doi:10.1016/j.nanoen.2019.02.002

Wu, X., Trinh, M. T., and Zhu, X.-Y. (2015). Excitonic Many-Body Interactions in Two-Dimensional Lead Iodide Perovskite Quantum Wells. *J. Phys. Chem. C* 119 (26), 14714–14721. doi:10.1021/acs.jpcc.5b00148

Xu, Q., Meng, K., Liu, Z., Wang, X., Hu, Y., Qiao, Z., et al. (2019). Synergistic Improvements in Efficiency and Stability of 2D Perovskite Solar Cells with Metal Ion Doping. *Adv. Mater. Inter.* 6 (23), 1901259. doi:10.1002/admi.201901259

Xu, Y., Wang, M., Lei, Y., Ci, Z., and Jin, Z. (2020). Crystallization Kinetics in 2D Perovskite Solar Cells. *Adv. Energ. Mater.* 10, 2002558. doi:10.1002/aenm.202002558

Yang, S., Wang, Y., Liu, P., Cheng, Y.-B., Zhao, H. J., and Yang, H. G. (2016). Functionalization of Perovskite Thin Films with Moisture-Tolerant Molecules. *Nat. Energ.* 1 (2). doi:10.1038/nenergy.2015.16

Zheng, F., Chen, W., Bu, T., Ghiggino, K. P., Huang, F., Cheng, Y., et al. (2019). Triggering the Passivation Effect of Potassium Doping in Mixed-Cation Mixed-Halide Perovskite by Light Illumination. *Adv. Energ. Mater.* 9 (24), 1901016. doi:10.1002/aenm.201901016

Zheng, F., Zuo, C., Niu, M., Zhou, C., Bradley, S. J., Hall, C. R., et al. (2020a). Revealing the Role of Methylammonium Chloride for Improving the Performance of 2D Perovskite Solar Cells. *ACS Appl. Mater. Inter.* 12 (23), 25980–25990. doi:10.1021/acsami.0c05714

Zheng, H. L., Liu, D. T., Wang, Y. F., Yang, Y. G., Li, H., Zhang, T., et al. (2020b). Synergistic Effect of Additives on 2D Perovskite Film towards Efficient and Stable Solar Cell. *Chem. Eng. J.* 389, 9. doi:10.1016/j.cej.2020.124266

Conflict of Interest: The authors declare that the research was conducted in the absence of any commercial or financial relationships that could be construed as a potential conflict of interest.